ADVANCED OPTICAL MATERIALS
www.advopticalmat.de

Near-Ultraviolet Structural Colors Generated by Aluminum Nanodisk Array for Bright Image Printing

*Chun-Ho Lee, Youngrok Kim, Jung-Hwan Song, Ho-Seok Ee, Min-Soo Hwang, Kwang-Yong Jeong, Hong-Gyu Park, Takhee Lee, and Min-Kyo Seo**

Structural colors generated by optical micro- or nanostructures have attracted much attention for replacing pigment colors due to their tunability and semipermanency. The advantages of structural colors are now ready to be extended to the spectral range outside that of visible wavelengths. Here, bright structural colors are demonstrated in the near-ultraviolet (near-UV) wavelength range based on the plasmonic resonance of an aluminum nanodisk array. Collective plasmonic oscillation of the aluminum nanodisks selectively reflects the near-UV light with a high reflectance and narrow linewidth. The color of the reflected light is tuned over the full near-UV range, depending on the structural parameters of the nanodisk array. In particular, aluminum nanodisk arrays can be used as structural color pixels that demonstrate printing of near-UV images with a high resolution of ≈10 000 pixels per inch. The demonstrated near-UV structural colors show significant progress toward UV filtering and imaging, anticounterfeit, color multiplexing, and photocatalysis.

Structural color generation based on the resonant reflection or transmission of optical nanostructures has been widely investigated as an excellent alternative to conventional pigment-based color generation.[1–3] Typically, pigments produce a color with a fixed spectrum determined by their inherent light absorption characteristics. On the other hand, structural color can be effectively tuned by changing the size and shape of the employed components, or the refractive index of the surrounding medium. Optical resonances of metallic or dielectric nanostructures and their interference in the organized arrangement or amorphous ensemble allow bright structural colors,[4–13] which can be actively controlled by mechanical deformation,[14,15] transient liquid crystals,[16–18] and electro- or thermochromic polymers.[19–21] In addition, a structural color is semipermanent unless its internal structure is destroyed or disrupted, while a pigment-based color suffers from photodegradation and oxidation in a real environment. These advantages of structural colors have been employed in various applications in the visible and near-infrared wavelength regions, including color pixels,[2,6–8] filters,[22–25] photodetectors,[26] filterless image sensors,[27] and sensitive biodetectors.[13]

Resonant reflection of ultraviolet (UV) light has been demonstrated using 3D photonic crystals[28] and multilayer structures.[29] Aluminum is one of the most promising materials to support plasmonic resonances not only in the visible region but also in the near-UV region. Structural color generation in the visible wavelength based on aluminum nanostructures has been reported.[6–10,30,31] However, a thin resonant reflection film employing plasmonic aluminum nanostructures, the center wavelength of which can be tuned over the full near-UV wavelength region, and its applications to UV structural color generation and image printing have not yet been reported. Optical resonances in the UV regime have been conventionally applied to enhance photocatalysis,[32] photoelectron emission,[33] and photoluminescence.[34,35] UV structural color materials are expected to be highly useful not only for the typical applications of UV optical resonances, but also for other further applications including colorization of UV images, anticounterfeiting,[36] visible-blind image sensing,[37] and dense color multiplexing.[38] We also note that aluminum-based structural colors can be seamlessly used as ultrathin filters to improve current devices for UV detection and imaging.[22,23,26]

In this work, we demonstrated bright reflective near-UV structural color generation based on the plasmonic resonance of an aluminum nanodisk array. Aluminum, of which the interband transition exists at a wavelength of ≈800 nm, exhibits lower material loss[39] and better performance in the UV wavelength

C.-H. Lee, Dr. J.-H. Song, Dr. H.-S. Ee, Prof. M.-K. Seo
Department of Physics and Institute for the NanoCentury
Korea Advanced Institute of Science and Technology (KAIST)
Daejeon 34141, Republic of Korea
E-mail: minkyo_seo@kaist.ac.kr
Y. Kim, Prof. T. Lee
Department of Physics and Astronomy
Institute of Applied Physics
Seoul National University (SNU)
Seoul 08826, Republic of Korea
Dr. H.-S. Ee, Dr. M.-S. Hwang, Prof. H.-G. Park
Department of Physics
Korea University (KU)
Seoul 02841, Republic of Korea
Prof. K.-Y. Jeong
Department of Nano Science and Technology
Gachon University
Gyeonggi-do 13120, Republic of Korea
The ORCID identification number(s) for the author(s) of this article can be found under https://doi.org/10.1002/adom.201800231.

DOI: 10.1002/adom.201800231

range than noble metals.[40–42] In addition, aluminum is compatible with the complementary metal–oxide–semiconductor (CMOS) process and suitable for mass production.[30,31,43] By controlling the geometry of the aluminum nanodisk array, the generated UV structural color was efficiently tuned over the full near-UV range. We finally demonstrated UV structural color pixels, check-patterned images, and an anticounterfeit image showing distinct responses to UV and visible illumination. The numerical simulation using the finite-difference time-domain (FDTD) method successfully reproduced the properties of the generated near-UV structural color, including the center wavelength, reflectance, and spectral width.

Bright structural color generation requires resonant reflection or transmission. Periodically arranged metal nanodisks support a narrow and strong optical resonance in reflection, due to coupling between the grating diffraction of the array and the plasmonic resonance of the individual nanodisk.[44,45] By controlling its resonance wavelength, the aluminum nanodisk array selectively reflects UV light but transmits visible light, as illustrated in **Figure 1**a. In optical microscope images (insets of Figure 1a), the fabricated aluminum nanodisk array, the resonance wavelength of which is ≈328 nm, is clearly observed under UV illumination (326 ± 12.5 nm), but is nearly indistinguishable from the bare substrate under visible illumination (halogen tungsten lamp). Here, the diameter and thickness of the nanodisk are 72 and 35 nm, respectively, and the period of the square lattice array is 190 nm. The numerical simulation results in Figure 1b indicate that, at the UV wavelength of 326 nm, the strongly reflected light interferes with the incident light and forms a standing wave pattern along the vertical direction. Plasmonic resonance highly concentrates the electric field of the incident UV light with an intensity enhancement of ≈71.6 at the maximum. On the other hand, visible incident light with a wavelength of 420 nm does not interact significantly with the aluminum nanodisk array, and the reflection of the array differs little from that of the bare substrate (Figure 1c).

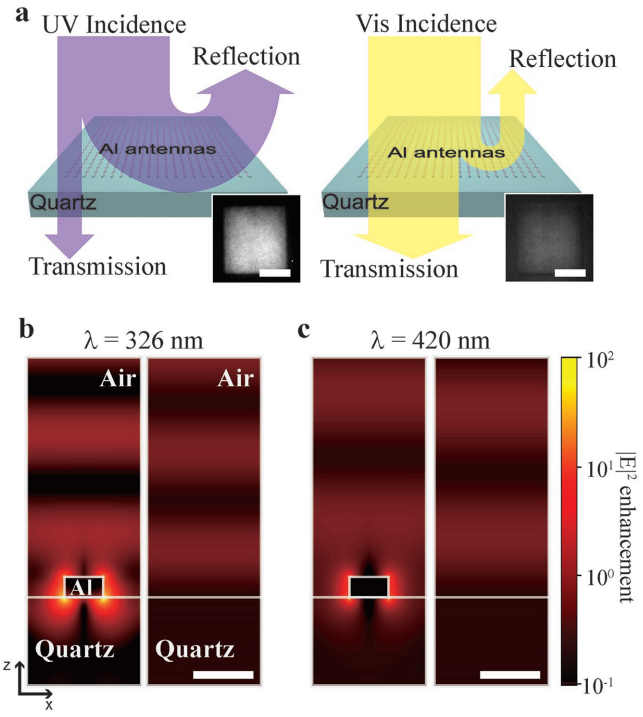

Figure 1. a) Schematic diagram of reflecting near-ultraviolet (UV) structural color generated by the aluminum nanodisk array. The collective plasmonic oscillation of the aluminum nanodisks selectively and strongly reflects UV light but transmits visible light. The insets show measured bright-field microscope images of an aluminum nanodisk array, of which the center wavelength of resonance is ≈328 nm, under near-UV (326 ± 12.5 nm) and visible (tungsten-halogen lamp) illuminations. Scale bar, 10 μm. b,c) Calculated electric field intensity distributions (log-scale) of the aluminum nanodisk array and the quartz substrate under 326 and 420 nm wavelength incidences, respectively. The field intensity is normalized to that of the incident light. Scale bar, 100 nm.

To characterize UV structural color generation, we measured the reflectance spectra of the aluminum nanodisk arrays. **Figure 2**a shows scanning electron microscope (SEM) images of the fabricated square lattice arrays of aluminum nanodisks on the quartz substrate. Aluminum nanodisk arrays (thickness: ≈35 nm) were fabricated using conventional electron beam lithography (EBL) followed by thermal evaporation and lift-off processes. While the filling factor, defined as the ratio of the physical area of the nanodisk to the unit cell area, was fixed at ≈11%, we changed the diameter of the nanodisk and the period of the square lattice from ≈74 to ≈94 nm and from ≈190 to ≈260 nm, respectively. The incident UV light from the deuterium lamp illuminates the nanodisk array through a UV objective lens (× 40; numerical aperture, NA: 0.5) and a linear polarizer. The illuminating area has a circular shape with a radius of ≈30 μm, sufficient for uniform coverage of the entire nanodisk array (size: 20 × 20 μm^2).

Figure 2b shows that as the scale of the nanodisk array increases, the resonance wavelength (λ_{res}) gradually increases from ≈323 to ≈400 nm (≈328 to ≈404 nm) for *x*-polarized (*y*-polarized) incidence. The slight difference between *x*- and *y*-polarizations is due to fabrication imperfections of the square lattice array. Over the near-UV range, we achieved high reflectance values of ≈30.8% (≈31.3%) for *x*-polarized (*y*-polarized) incidence on average at resonance, despite the low filling ratio. In the off-resonance region, the reflectance is ≈5%, which corresponds to that of the quartz substrate. The resonant behavior with a narrow linewidth, of which the average full width at half maximum (FWHM) is ≈0.174λ_{res} (≈0.170λ_{res}) for *x*-polarized (*y*-polarized) incidence, enables UV structural color generation. We note that the peak reflectance and FWHM of the UV resonance are compatible with those of visible structural colors in previous reports.[1,4] The distinct resonance in the reflection spectrum originates from collective plasmonic oscillation due to the near-field coupling of the nanodisks.[44–46]

To understand the resonant UV structural color generation, we calculated the reflectance spectra under the normally incident planewave using the FDTD method employing the periodic boundary condition (Figure 2c). The diameter of the Al nanodisk and the period of the square lattice are identical to those of the experiments. In the FDTD simulation, we used the Drude model to fit the experimental permittivity of Al in the spectral range from 250 to 450 nm[39] (Table S1, Supporting Information). The refractive index of the quartz substrate is fixed to 1.56. The simulation reproduces the resonance wavelength and its shift in the experiment depending on the scale

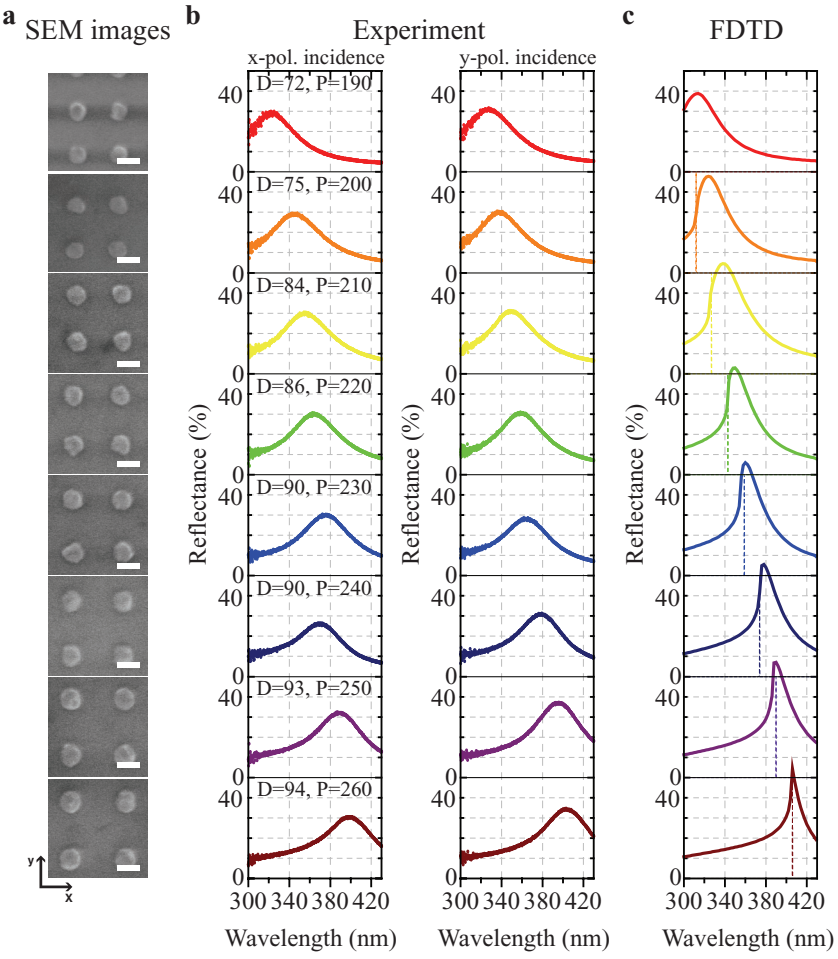

Figure 2. a) Scanning electron microscope (SEM) images of the fabricated aluminum nanodisk arrays. Scale bar, 100 nm. The thickness of a nanodisk is ≈35 nm, by atomic force microscopy measurements. b) Measured reflectance spectra of the aluminum nanodisk arrays in Figure 2a. The diameter of the nanodisk, *D*, and the period of the square lattice array, *P*, change with fixing of the filling ratio of the disk to the unit cell. c) Calculated reflectance spectra under normally incident near-UV light. The dashed vertical lines indicate the spectral positions of the Rayleigh–Wood anomaly. The simulation grid size is 2 nm.

of the nanodisk array. We note that the absorption spectrum shows a similar behavior as the reflectance spectrum and the transmittance exhibits an opposite behavior to the reflectance and absorption (Figure S1, Supporting Information). The transmittance becomes higher than 80% at off resonance, which shows that the aluminum nanodisk array can also be useful to generate complementary, transmissive structural color with a high contrast ratio.

Compared with the experimental results, the calculated resonances have higher peak reflectance values and narrower FWHMs and exhibit asymmetric line shapes due to the Fano-like interference between the Rayleigh–Wood anomaly mode and plasmonic resonance.[47–49] This is because, in the experiments, the incident (reflected) light was focused (collected) with a divergence angle of ±30° corresponding to the NA of the objective lens. Plasmonic resonance and the Rayleigh–Wood anomaly of the aluminum nanodisk array are sensitive to the angle of incidence and reflected radiation (Figure S2, Supporting Information). The focusing and collection of light with a divergence angle broaden and blur the narrow, asymmetric line shape of the reflection resonance. In addition, fabrication errors in the diameters and positions of the aluminum disks can cause inhomogeneous broadening of the resonance spectrum. We also examined the effects of extra damping of the nanostructured aluminum with a larger collision frequency than that of the bulk aluminum. The larger the damping causes a lower reflectance and slightly shorter center wavelength, but the shape of the reflectance spectrum does not change much (Figure S3, Supporting Information). We note that the thin native oxide layer on the surface of aluminum may degrade the performance of plasmonic aluminum nanostructures in the UV wavelength range.[41] We calculated the effects of the thin aluminum oxide layer on the reflectance spectrum. The thin surface oxide layer lowers the peak reflectance but does not change the shape of the resonant reflectance spectrum much (Figure S4, Supporting Information). It has been reported that a transparent UV-curable organic–inorganic hybrid material coating will protect not only from severe oxidation but also from mechanical damage or greasy contamination.[43] To avoid further significant oxidation, we kept the samples in a vacuum chamber except during the measurement. To examine the long-term stability of the aluminum nanodisk array, we measured the same aluminum nanodisk arrays again one and a half years later than the measurement in Figure 2b. We have kept the samples in ambient condition after the first measurement. We successfully confirmed that the reflectance spectra of the first and second measurements are almost same despite such a long period (Figure S5, Supporting Information).

Calculating angle- and polarization-dependent reflectance spectrum of an aluminum nanodisk array under oblique incident planewave, we examine the effects of the Rayleigh–Wood anomalies on the structural color generation (**Figure 3**). We employed the Bloch boundary condition in the FDTD simulation and calculated the power ratio between the reflected light to air and the incident light. The angle of incidence varies from 0° to 45° with a step of 5°. The nanodisk array with a period of 230 nm shows both of the Rayleigh–Wood anomalies in the quartz substrate ($n = 1.56$) and air ($n = 1$) in the near-UV region. As the incident angle increases, the Rayleigh–Wood anomaly condition shifts to longer wavelengths and causes a significant effect on the structural color characteristics. The abnormal resonances indicated by the black arrows in Figure 3 are due to the anticrossing coupling between the plasmonic resonance of the aluminum nanodisk and the Rayleigh–Wood anomalies.[50] At an incident angle smaller than 20°, the reflectance spectra for both P- and S-polarization show similar behavior, but

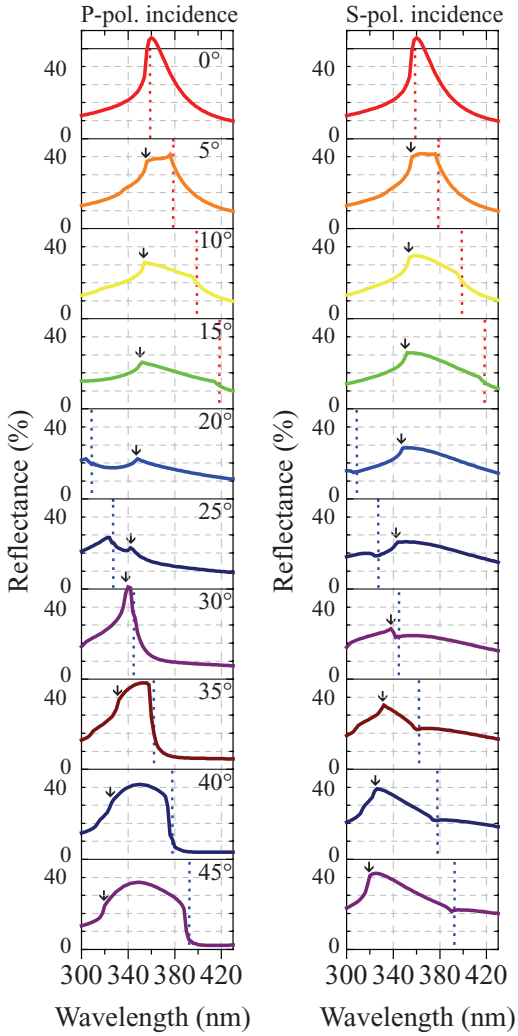

Figure 3. Calculated reflectance spectra depending on the angle of incidence for P- (left) and S-polarization (right). The angle of incidence varies from 0° to 45°. We examine the array of which the nanodisk diameter and period are 90 and 230 nm, respectively. The red and blue dotted lines indicate the conditions of the Rayleigh–Wood anomaly in the substrate ($n = 1.56$) and air ($n = 1$), respectively. The black arrow indicates the abnormal resonance due to the anticrossing coupling between the plasmonic resonance of the aluminum nanodisk and the Rayleigh–Wood anomalies. The simulation grid size is 2 nm.

approaching Brewster's angle (57.3°), the oblique incidence provides a background off-resonance reflectance for P-polarization much weaker than that for S-polarization. Practical application of structural colors requires insensitive dependence on the incident angle and polarization. It has been reported that introduction of randomness to the periodic structure[4] and hybridization of two different plasmonic modes[43] can improve the angle- and polarization-dependent performance of structural colors based on nano-optical resonances.

Figure 4 shows the measured bright-field microscope images of the aluminum nanodisk arrays under various UV illuminations through different bandpass filters, of which the center wavelength/FWHM values are 326/25, 340/25, 365/25, 380/10, 400/25, and 420/20 nm, respectively (Figure S6, Supporting Information). Here, we determined the reflectance of the array by a relative comparison with that of the bare quartz substrate. The resonant characteristics produce structural colors sensitive to the spectral window of the bandpass filter, and tunable over the full near-UV region while keeping the brightness to ≈35% around the resonance wavelength. Thus, the eight near-UV structural color arrays were successfully distinguished from each other. It is also worth noting that the filling factor of ≈11% is sufficient to generate uniform reflection over the entire nanodisk array as the period of the array is smaller than the Abbe limit.

Finite-sized arrays of aluminum nanodisks can act as structural color pixels to print UV images. **Figure 5**a shows SEM images of two arrays, of which the period and nanodisk diameter (P, D) are 190 and 62 nm, and 250 and 86 nm, respectively. As shown in Figure 5b, the two nanodisk arrays have different resonance wavelengths of ≈317 and ≈387 nm, but almost the same peak reflectance values of ≈21.1% and ≈20.7%. Due to their smaller filling factors of ≈8%, the aluminum nanodisk arrays in Figure 5 exhibit lower reflectance values than the arrays in Figure 2. When demonstrating a structural color pixel using the finite-sized array, it should be noted that the brightness of the array depends on its size.[51] Figure 5c shows simulated reflection spectra of the finite-sized arrays with different numbers of nanodisks (3 × 3, 5 × 5, and 11 × 11 nanodisk arrays) and the infinite array.

We calculated an effective reflectance, defined by the integrated flux ratio between the incident and reflected light. The fluxes of the incident and reflected light are integrated over the area of the finite-sized array, which is determined by the area of the unit cell times the number of unit cells. As the size of the array increases, the brightness increases, the spectral width becomes narrower and, finally, the reflective spectrum gradually approaches that of the infinite array. This is because the near-field coupling with neighboring nanodisks enables the aluminum nanodisk to reflect the incident light to air to a greater degree than the uncoupled single nanodisk.[1] On the other hand, the nanodisk array exhibits a lower transmittance than the single nanodisk, as the scattered field by the coupled nanodisks interferes destructively with the incident field in the substrate (Figure S7, Supporting Information). At the edge of the array, a relatively small number of nanodisks interact, and the near-field coupling becomes weak; the smaller the array, the lower the reflectance due to the edge effect. However, the arrays with 5 × 5 nanodisks, of which the physical sizes are only in the order of 1 × 1 μm^2, are sufficient to demonstrate bright UV structural color pixels.

We demonstrate two-tone check pattern images using two UV structural color pixels. Figure 5d shows bright-field reflective microscope images of four check patterns with different pixel sizes under bandpass filtered near-UV illumination. As the center wavelength of the near-UV illumination changes, the bright and dark areas reverse at a wavelength of 350 nm. The pixel sizes of the check patterns are 10.0, 5.0, 2.5, and 1.0 μm on a side, respectively. The pixels with a size of 2.5 μm not only support an ultrahigh resolution of ≈10 000 pixels per inch (PPI), but also generate a clear checkered-patterned near-UV image without undesired color mixing between pixels. We note that the typical industry standard for excellent printing

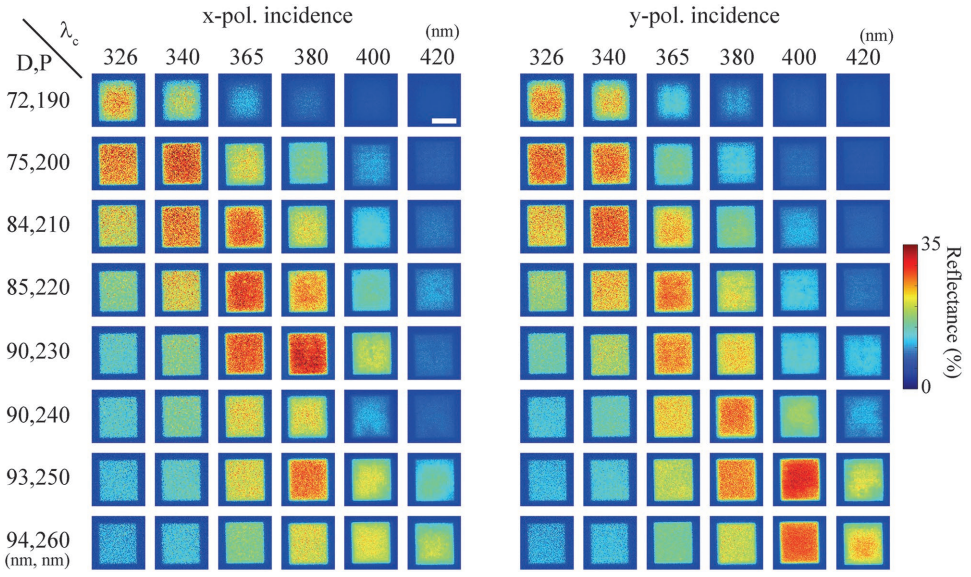

Figure 4. Bright-field microscope images of the aluminum nanodisk arrays under the different illuminations through 326/25, 340/25, 365/25, 380/10, 400/25, and 420/20 nm bandpass filters. The bandpass filters were used to mimic the role of the visual cell in the near-UV range. Scale bar, 10 μm.

quality is >300 PPI. As predicted by the FDTD simulations (Figure 5c), the smaller the pixel size, the lower the contrast between the bright and dark areas. However, although the contrast becomes low, the smallest pixel with a size of 1 μm also produces a distinct two-tone check pattern and exhibits distinct reversal of the bright and dark areas.

As a unique application of the bright near-UV image printing, we demonstrated an anticounterfeit image of the

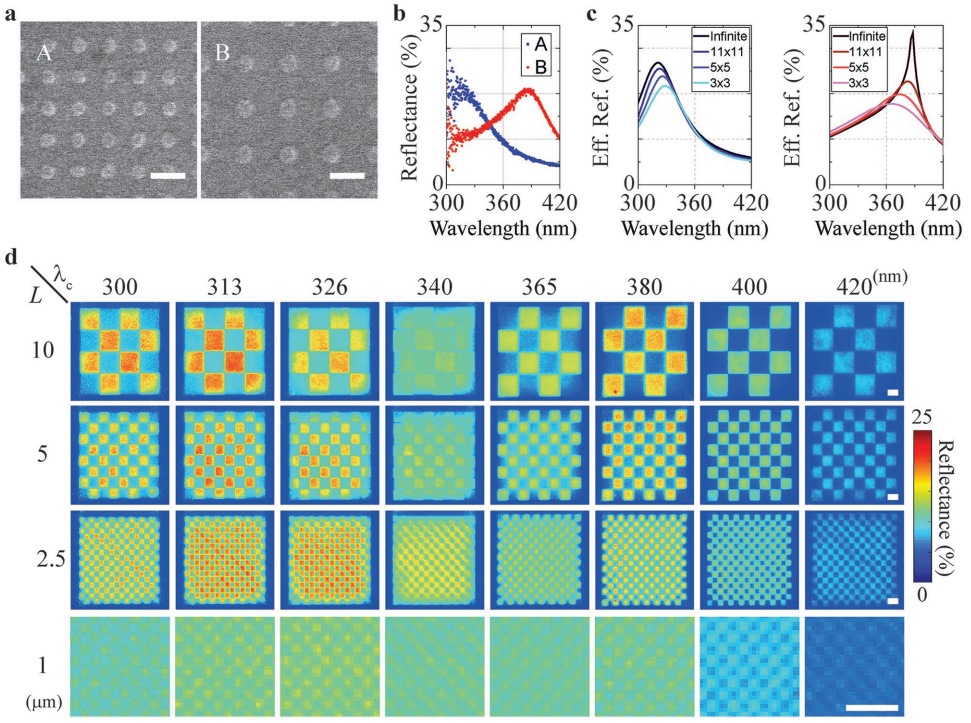

Figure 5. a) SEM images of two different aluminum nanodisk arrays, A (left) and B (right) with a diameter and period of 62 and 190 nm, and 86 and 250 nm, respectively. Scale bar denotes 200 nm. b) Measured reflectance spectra of the two arrays, the areas of which are identical to 10×10 μm^2. c) Calculated effective reflectance spectra of the two arrays depending on the pixel size. We simulated the finite-sized arrays containing 3×3, 5×5, and 11×11 nanodisks, as well as the infinite array. The simulation grid size is 4 nm. d) Bright-field microscope images of the check pattern consisting of two nanodisk arrays under near-UV illumination through 300/25, 313/25, 326/25, 340/25, 365/25, 380/10, 400/25, and 420/20 nm bandpass filters. Here, *L* is the size of the pixel on a given side. Scale bar, 5 μm.

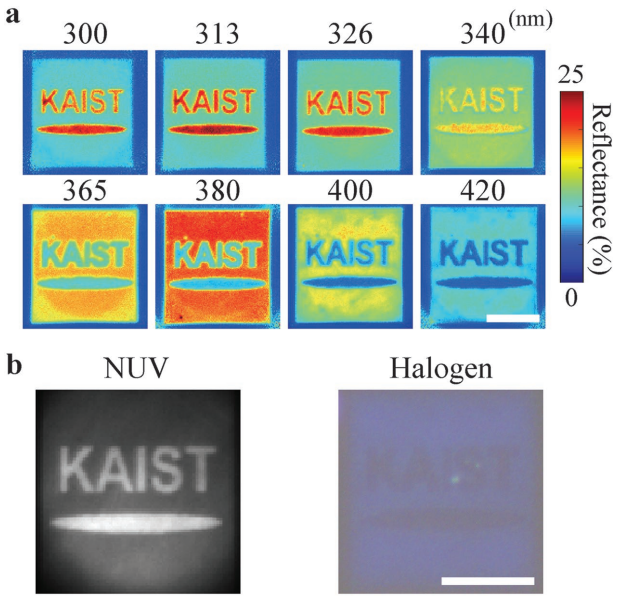

Figure 6. a) Bright-field microscope images of the KAIST logo under illumination through 300/25, 313/25, 326/25, 340/25, 365/25, 380/10, 400/25, and 420/20 nm bandpass filters. Scale bar, 20 μm. b) Application of near-UV structural colors to anticounterfeit image printing. The anticounterfeit printing shows distinct bright-field reflection images under the UV (313 ± 12.5 nm) and visible (tungsten-halogen lamp) illumination. Scale bar, 20 μm.

KAIST logo with a size of 40 × 40 μm^2 (**Figure 6**). The bright-field microscope images under different near-UV illuminations in Figure 6a show the distinct behaviors of the background and logo, which consist of different near-UV structural colors. The logo and background areas were filled by the aluminum nanodisk arrays, as shown in Figure 5a. The printed logo changes from an embossed image to an engraved image as the wavelength of the UV illumination increases. Above all, the image of the logo is clearly distinguished under near-UV illumination (313 ± 12.5 nm) but is hardly distinguishable under visible illumination (halogen tungsten lamp), as shown in Figure 6b. Compared with conventional fluorescence-based anticounterfeit image printing,[52] this UV structural color-based anticounterfeit image is permanent, and easy to create and detect. Moreover, the combination of the near-UV structural colors with different reflectance spectra provides a more complex and powerful anticounterfeiting method.

In summary, we demonstrated reflecting structural colors in the near-UV wavelength range using aluminum nanodisk arrays. The collective and distinct resonance of plasmonic aluminum nanodisks in the array generates bright near-UV structural colors, of which the center wavelength can be easily tuned depending on the diameter of the nanodisk and period of the array. The strong resonance phenomenon enables a high reflectance of more than 30%, even at a low filling ratio of ≈11%. The FDTD simulations successively reproduced the resonant reflection spectrum and its size-dependent behavior. Employing the aluminum nanodisk array as a structural color pixel, we printed high-resolution UV images of over 10 000 PPI and demonstrated an anticounterfeit image, which behaves completely different under near-UV and visible illumination. We expect that the near-UV structural color medium will be highly useful for various applications, including ultrathin CMOS-compatible filters for UV detection and imaging, visible-blind image sensing, dense color multiplexing, and power-efficient photocatalysis.

Experimental Section

Fabrication: The aluminum nanodisk arrays were fabricated using typical EBL, followed by thermal evaporation and lift-off processes. A poly(methyl methacrylate) (PMMA) positive electron beam resist layer was spin-coated on the quartz substrate. A conductive polymer (Espacer 300Z, Showa Denko) layer, additionally coated on the PMMA layer, reduces the charging effect during the EBL process. The EBL patterns were developed by 1:3 methyl isobutyl ketone:isopropyl alcohol solution for 40 s at 25 °C. A 35 nm thick thermally evaporated aluminum layer was deposited with a rate of 0.5 Å s^{-1}, and a lift-off process with a solvent stripper (Remover PG) at 80 °C was followed.

Supporting Information

Supporting Information is available from the Wiley Online Library or from the author.

Acknowledgements

M.-K.S. acknowledged support of this work by National Research Foundation of Korea (NRF) (Nos. 2017R1A4A1015426, 2017R1A2B2009117, 2016R1D1A1B03935938, 2014M3C1A3052537, and 2014M3A6B3063709). H.-G.P. acknowledges the support by NRF (No. 2009-0081565). T.L. acknowledges support by the National Creative Research Laboratory program (Grant No. 2012026372) of NRF.

Conflict of Interest

The authors declare no conflict of interest.

Keywords

image printing, near-ultraviolet, plasmonic nanostructures, structural color generation

Received: February 21, 2018
Revised: April 13, 2018
Published online: May 31, 2018

[1] W. Zhou, T. W. Odom, *Nat. Nanotechnol.* **2011**, *6*, 423.
[2] K. Kumar, H. G. Duan, R. S. Hegde, S. C. W. Koh, J. N. Wei, J. K. W. Yang, *Nat. Nanotechnol.* **2012**, *7*, 557.
[3] A. Kristensen, J. K. W. Yang, S. I. Bozhevolnyi, S. Link, P. Nordlander, N. J. Halas, N. A. Mortensen, *Nat. Rev. Mater.* **2016**, *2*, 16088.
[4] K. Chung, S. Yu, C. J. Heo, J. W. Shim, S. M. Yang, M. G. Han, H. S. Lee, Y. Jin, S. Y. Lee, N. Park, J. H. Shin, *Adv. Mater.* **2012**, *24*, 2375.
[5] A. S. Roberts, A. Pors, O. Albrektsen, S. I. Bozhevolnyi, *Nano Lett.* **2014**, *14*, 783.
[6] S. J. Tan, L. Zhang, D. Zhu, X. M. Goh, Y. M. Wang, K. Kumar, C. W. Qiu, J. K. Yang, *Nano Lett.* **2014**, *14*, 4023.

[7] J. Olson, A. Manjavacas, L. Liu, W. S. Chang, B. Foerster, N. S. King, M. W. Knight, P. Nordlander, N. J. Halas, S. Link, *Proc. Natl. Acad. Sci. USA* **2014**, *111*, 14348.
[8] X. M. Goh, Y. Zheng, S. J. Tan, L. Zhang, K. Kumar, C. W. Qiu, J. K. Yang, *Nat. Commun.* **2014**, *5*, 5361.
[9] F. Cheng, X. Yang, D. Rosenmann, L. Stan, D. Czaplewski, J. Gao, *Opt. Express* **2015**, *23*, 25329.
[10] M. Keshavarz Hedayati, M. Elbahri, *Plasmonics* **2017**, *12*, 1463.
[11] J. Xue, Z. K. Zhou, Z. Wei, R. Su, J. Lai, J. Li, C. Li, T. Zhang, X. H. Wang, *Nat. Commun.* **2015**, *6*, 8906.
[12] Y. Gu, L. Zhang, J. K. Yang, S. P. Yeo, C. W. Qiu, *Nanoscale* **2015**, *7*, 6409.
[13] M. Elbahri, M. Abdelaziz, S. Homaeigohar, A. Elsharawy, K. Hedayati, C. Röder, M. El Haj Assad, R. Abdelaziz, *Adv. Mater.* **2018**, *30*, 1704442.
[14] J. Teyssier, S. V. Saenko, D. van der Marel, M. C. Milinkovitch, *Nat. Commun.* **2015**, *6*, 6368.
[15] M. L. Tseng, J. Yang, M. Semmlinger, C. Zhang, P. Nordlander, N. J. Halas, *Nano Lett.* **2017**, *17*, 6034.
[16] Y. Jiang, D. Xu, X. S. Li, C. X. Lin, W. N. Li, Q. An, C. A. Tao, H. Tang, G. T. Li, *J. Mater. Chem.* **2012**, *22*, 11943.
[17] D. Franklin, Y. Chen, A. Vazquez-Guardado, S. Modak, J. Boroumand, D. Xu, S.-T. Wu, D. Chanda, *Nat. Commun.* **2015**, *6*, 7337.
[18] J. Olson, A. Manjavacas, T. Basu, D. Huang, A. E. Schlather, B. Zheng, N. J. Halas, P. Nordlander, S. Link, *ACS Nano* **2016**, *10*, 1108.
[19] K. Ueno, J. Sakamoto, Y. Takeoka, M. Watanabe, *J. Mater. Chem.* **2009**, *19*, 4778.
[20] T. Xu, E. C. Walter, A. Agrawal, C. Bohn, J. Velmurugan, W. Zhu, H. J. Lezec, A. A. Talin, *Nat. Commun.* **2016**, *7*, 10479.
[21] K. Xiong, D. Tordera, G. Emilsson, O. Olsson, U. Linderhed, M. P. Jonsson, A. B. Dahlin, *Nano Lett.* **2017**, *17*, 7033.
[22] S. Yokogawa, S. P. Burgos, H. A. Atwater, *Nano Lett.* **2012**, *12*, 4349.
[23] S. P. Burgos, S. Yokogawa, H. A. Atwater, *ACS Nano* **2013**, *7*, 10038.
[24] V. R. Shrestha, S. S. Lee, E. S. Kim, D. Y. Choi, *Nano Lett.* **2014**, *14*, 6672.
[25] L. Duempelmann, A. Luu-Dinh, B. Gallinet, L. Novotny, *ACS Photonics* **2016**, *3*, 190.
[26] B. Y. Zheng, Y. Wang, P. Nordlander, N. J. Halas, *Adv. Mater.* **2014**, *26*, 6318.
[27] H. Park, Y. Dan, K. Seo, Y. J. Yu, P. K. Duane, M. Wober, K. B. Crozier, *Nano Lett.* **2014**, *14*, 1804.
[28] A. M. Urbas, M. Maldovan, P. DeRege, E. L. Thomas, *Adv. Mater.* **2002**, *14*, 1850.
[29] F. Song, H. L. Su, J. J. Chen, D. Zhang, W. J. Moon, *Appl. Phys. Lett.* **2011**, *99*, 163705.
[30] X. Zhu, C. Vannahme, E. Hojlund-Nielsen, N. A. Mortensen, A. Kristensen, *Nat. Nanotechnol.* **2016**, *11*, 325.
[31] E. Højlund-Nielsen, J. Clausen, T. Mäkela, L. H. Thamdrup, M. Zalkovskij, T. Nielsen, N. Li Pira, J. Ahopelto, N. A. Mortensen, A. Kristensen, *Adv. Mater. Technol.* **2016**, *1*, 1600054.
[32] M. Honda, Y. Kumamoto, A. Taguchi, Y. Saito, S. Kawata, *Appl. Phys. Lett.* **2014**, *104*, 061108.
[33] Y. Watanabe, W. Inami, Y. Kawata, *J. Appl. Phys.* **2011**, *109*, 023112.
[34] S. K. Jha, N. Mojarad, M. Agio, J. F. Loffler, Y. Ekinci, *Opt. Express* **2015**, *23*, 24719.
[35] A. Kannegulla, Y. Liu, B. Wu, L.-J. Cheng, *Appl. Phys. Lett.* **2017**, *111*, 081106.
[36] A. F. Smith, P. Patton, S. E. Skrabalak, *Adv. Funct. Mater.* **2016**, *26*, 1315.
[37] E. Cicek, Z. Vashaei, E. K.-w. Huang, R. McClintock, M. Razeghi, *Opt. Lett.* **2012**, *37*, 896.
[38] Y. W. Huang, W. T. Chen, W. Y. Tsai, P. C. Wu, C. M. Wang, G. Sun, D. P. Tsai, *Nano Lett.* **2015**, *15*, 3122.
[39] D. R. Lide, *CRC Handbook of Chemistry and Physics*, CRC Press, Boca Raton, FL **2006**.
[40] M. W. Knight, L. Liu, Y. Wang, L. Brown, S. Mukherjee, N. S. King, H. O. Everitt, P. Nordlander, N. J. Halas, *Nano Lett.* **2012**, *12*, 6000.
[41] M. W. Knight, N. S. King, L. Liu, H. O. Everitt, P. Nordlander, N. J. Halas, *ACS Nano* **2014**, *8*, 834.
[42] K. Thyagarajan, C. Santschi, P. Langlet, O. J. F. Martin, *Adv. Opt. Mater.* **2016**, *4*, 871.
[43] J. S. Clausen, E. Højlund-Nielsen, A. B. Christiansen, S. Yazdi, M. Grajower, H. Taha, U. Levy, A. Kristensen, N. A. Mortensen, *Nano Lett.* **2014**, *14*, 4499.
[44] S. Zou, N. Janel, G. C. Schatz, *J. Chem. Phys.* **2004**, *120*, 10871.
[45] B. Auguié, W. L. Barnes, *Phys. Rev. Lett.* **2008**, *101*, 143902.
[46] V. G. Kravets, F. Schedin, A. N. Grigorenko, *Phys. Rev. Lett.* **2008**, *101*, 087403.
[47] B. Lamprecht, G. Schider, R. T. Lechner, H. Ditlbacher, J. R. Krenn, A. Leitner, F. R. Aussenegg, *Phys. Rev. Lett.* **2000**, *84*, 4721.
[48] Y. Z. Chu, E. Schonbrun, T. Yang, K. B. Crozier, *Appl. Phys. Lett.* **2008**, *93*, 181108.
[49] B. Auguié, X. M. Bendaña, W. L. Barnes, F. J. García de Abajo, *Phys. Rev. B* **2010**, *82*, 155447.
[50] S. R. K. Rodriguez, A. Abass, B. Maes, O. T. A. Janssen, G. Vecchi, J. Gómez Rivas, *Phys. Rev. X* **2011**, *1*, 021019.
[51] S. R. K. Rodriguez, M. C. Schaafsma, A. Berrier, J. G. Rivas, *Physica B* **2012**, *407*, 4081.
[52] J. Andres, R. D. Hersch, J.-E. Moser, A.-S. Chauvin, *Adv. Funct. Mater.* **2014**, *24*, 5029.